Electronic band structure of a type-II 'W' quantum well calculated by an eight-band $\boldsymbol{k}\cdot\boldsymbol{p}$ model*

Yu Xiu(迂 修)[a], Gu Yong-Xian(谷永先)[b], Wang Qing(王 青)[a]†,
Wei Xin(韦 欣)[a], and Chen Liang-Hui(陈良惠)[a]

[a] *Nano-Optoelectronics Laboratory, Institute of Semiconductors, Chinese Academy of Sciences, Beijing* 100083, *China*
[b] *Key Laboratory of Semiconductor Materials, Institute of Semiconductors, Chinese Academy of Sciences, Beijing* 100083, *China*

(Received 31 August 2010; revised manuscript received 4 October 2010)

In this paper, we present an investigation of type-II 'W' quantum wells for the InAs/$Ga_{1-x}In_xSb$/AlSb family, where 'W' denotes the conduction profile of the material. We focus our attention on using the eight-band $\boldsymbol{k}\cdot\boldsymbol{p}$ model to calculate the band structures within the framework of finite element method. For the sake of clarity, the simulation in this paper is simplified and based on only one period—AlSb/InAs/$Ga_{1-x}In_xSb$/InAs/AlSb. The obtained numerical results include the energy levels and wavefunctions of carriers. We discuss the variations of the electronic properties by changing several important parameters, such as the thickness of either InAs or $Ga_{1-x}In_xSb$ layer and the alloy composition in $Ga_{1-x}In_xSb$ separately. In the last part, in order to compare the eight-band $\boldsymbol{k}\cdot\boldsymbol{p}$ model, we recalculate the conduction bands of the 'W' structure using the one-band $\boldsymbol{k}\cdot\boldsymbol{p}$ model and then discuss the difference between the two results, showing that conduction bands are strongly coupled with valence bands in the narrow band gap structure. The in-plane energy dispersions, which illustrate the suppression of the Auger recombination process, are also obtained.

Keywords: type-II 'W' quantum well, Burt-Foreman Hamiltonian, finite element methods
PACS: 05.65.tb, 73.21.Fg, 73.20.–r, 73.65.Ey **DOI:** 10.1088/1674-1056/20/3/030507

1. Introduction

Semiconductor lasers emitting in the 2–5 μm range have many applications, such as chemical detection, telecommunications and military counters.[1−3] There is currently an increasing demand for instruments working in this range. However, research in the mid-infrared (mid–IR) range has only been conducted in recent years due to difficulty in preparing the materials. Nowadays, many promising candidates operating in this range are well proposed, such as inter-band band cascade lasers (ICLs), inter-subband cascade lasers (QCLs), antimonide type-I and type-II quantum well (QW) lasers, and InAs/GaSb short-period supperlattices (SPSLs).[2−5] Quite recently, ICLs based on type-II 'W' active layers have been demonstrated to operate at room temperature with a wavelength of 3.75 μm and a continuous wave (cw) power output as high as 10 mW.[6] By contrast, antimonide type-II 'W' lasers based on one stage (non-cascade) remain the most outstanding among all of these candidates – although some problems still need to be solved.[7] The first type-II 'W' laser diode was proposed by Meyer *et al.*[8] in 1995, which was composed of four-constitute InAs/$Ga_{1-x}In_xSb$/InAs/$Ga_{1-x}Al_xSb$ multiple quantum wells. The so–called 'W' structure manifests the profile of the conduction band (CB), typically with one hole QW ($Ga_{1-x}In_xSb$) sandwiched between two electron QWs (InAs). The purpose of this configuration is to form two-dimensional electron and hole populations by improving the carrier confinement, and to enhance the optical coupling, as well as suppressing the Auger recombination rate.[8] There is no doubt that Auger recombination has always been a serious problem in designing semiconductor laser diodes, especially for long wavelength mid-IR range lasers. The type-II 'W' structure in an active region can effectively eliminate the non-radiative Auger process by removing the resonance between the energy gap and the split-off gap, which is usually dominant in many mid-IR materials. In the previous work, in almost all of these type-II 'W' structures the InAs-GaSb-AlSb family was used as the active region, and laser diodes based on a type-II 'W' configuration were investigated both experimentally and theoretically.[6−9]

In the present paper, we use the finite element method (FEM) to calculate the energy levels and wavefunction of the type-II 'W' structure within the framework of the eight-band $\boldsymbol{k}\cdot\boldsymbol{p}$ model

*Project supported by the National Natural Science Foundation of China (Grant No. 60636030).
†Corresponding author. E-mail: wangqing@mail.semi.ac.cn
© 2011 Chinese Physical Society and IOP Publishing Ltd

including strain. For simplicity, our simulation is based on only one period—a structure including five-constitute AlSb/InAs/$Ga_{1-x}In_xSb$/InAs/AlSb. Furthermore, we investigate the relationship between the fundamental band gap, which corresponds to wavelength and layer thickness (including 'electron' well layer and 'hole' well layer), and then draw the conclusion that as the thickness of the well layer increases, the wavelength becomes longer. By varying the alloy composition in $Ga_{1-x}In_xSb$, we also obtain a reasonable result that the wavelength becomes longer when 'In' composition increases. Finally we recalculate the conduction bands of the 'W' structure using the one-band $\boldsymbol{k}\cdot\boldsymbol{p}$ model. When compared to former results, some distinct consequences illustrate that conduction bands are strongly coupled with valence bands, especially for narrow band gap structures, which may not be totally ignored.

2. Theory

Discussed below is the eight-band $\boldsymbol{k}\cdot\boldsymbol{p}$ theory, which is based on the Kane theory, using the following set of basis functions:

$$\begin{aligned}&(|S\uparrow\rangle, |X\uparrow\rangle, |Y\uparrow\rangle, |Z\uparrow\rangle,\\ &|S\downarrow\rangle, |X\downarrow\rangle, |Y\downarrow\rangle, |Z\downarrow\rangle,)^{\mathrm{T}}\end{aligned} \tag{1}$$

and taking the block matrix form as follows:[10,11]

$$\boldsymbol{H} = \begin{pmatrix} \boldsymbol{G}(\boldsymbol{K}) & \boldsymbol{\Gamma} \\ -\bar{\boldsymbol{\Gamma}} & \bar{\boldsymbol{G}}(\boldsymbol{K}) \end{pmatrix}, \tag{2}$$

where $\boldsymbol{G}$ and $\boldsymbol{\Gamma}$ are both 4×4 matrices, with the matrix $\boldsymbol{G}$ being composed of four parts, i.e., $\boldsymbol{G}_1$, $\boldsymbol{G}_2$, $\boldsymbol{G}_{\mathrm{st}}$, which denote a potential energy, a kinetic energy and a strain dependent part, respectively, and $\boldsymbol{G}_{\mathrm{SO}}$, which describes spin orbit splitting, and with the matrix $\boldsymbol{\Gamma}$ also describing the spin orbit splitting; the overbar denotes the complex conjugation.

$$\boldsymbol{G} = \boldsymbol{G}_1 + \boldsymbol{G}_2 + \boldsymbol{G}_{\mathrm{SO}} + \boldsymbol{G}_{\mathrm{st}}, \tag{3}$$

where the four terms on the right-hand side are described in the appendix. We investigate the type-II 'W' quantum well band structure. The bulk 8×8 matrix can be converted into eight coupled differential equations by replacing k_z with $-\mathrm{i}\frac{\partial}{\partial z}$. According to the theory in Refs. [12] and [13], we replace the symmetrized matrix with an unsymmetrized matrix. The diagonal terms are treated as $Qk_i^2 = \hat{k}_i Q \hat{k}_i$, where Q is a Kane parameter, while the upper triangular matrix elements are no longer $Qk_ik_j \to \left(\hat{k}_iQ\hat{k}_j + \hat{k}_jQ\hat{k}_i\right)/2$, but described as $N'k_ik_j \to \hat{k}_iN_+\hat{k}_j + \hat{k}_jN_-\hat{k}_i$. Meanwhile, the lower triangular matrix elements $Qk_ik_j \to \left(\hat{k}_jQ\hat{k}_i + \hat{k}_iQ\hat{k}_j\right)/2$ are also replaced with $N'k_ik_j \to \hat{k}_jN_+\hat{k}_i + \hat{k}_iN_-\hat{k}_j$, where $N_- = M - \hbar^2/2m_0$ and $N_+ = N' - N_-$. Within the effective-mass approximation, the Schrödinger equation is given as

$$\hat{H}\,\Psi(z) = E\,\Psi(z). \tag{4}$$

In our calculation, $\phi(z)$ and $\varphi(z)$ represent the wavefuction and the envelop function, respectively, and expressed, respectively, as

$$\begin{aligned}\phi(z) = {} & u_1|S\uparrow\rangle + u_2|X\uparrow\rangle + u_3|Y\uparrow\rangle\\ & + u_4|Z\uparrow\rangle + u_5|S\downarrow\rangle + u_6|X\downarrow\rangle\\ & + u_7|Y\downarrow\rangle + u_8|Z\downarrow\rangle,\end{aligned} \tag{5}$$

and

$$\varphi(z) = \sum_{i=1}^{8} |u_i(z)|^2. \tag{6}$$

table 1 below shows the definitions of the parameters we used.

Table 1. Definitions of parameters.

E_0	fundamental band gap
E_{v}	valence band edge
E_{p}	optical matrix parameter
Δ	spin orbit splitting energy
$m_{\mathrm{e}}{}^*$	electron effective mass in conduction band
$\gamma 1, \gamma 2, \gamma 3$	three Luttinger parameters
a_{c}	hydrostatic conduction band deformation potential
a_{v}	hydrostatic valence band deformation potential
b_{v}	uniaxial ([100] direction) valence band deformation potential
d_{v}	uniaxial ([111] direction) valence band deformation potential

3. Results and discussion

In our simulation, the parameters are taken from Ref. [14]. The numerical results involve some spurious solutions. As we know, spurious solutions can be effectively eliminated by reducing $E_{\rm p}$ appropriately,[15,16] so we choose $E_{\rm p}$ (Table 2) a bit lower than that given in Ref. [14]. The first type-II 'W' structure devised by Meyer is composed of multiple quantum wells. By comparison, we use AlSb as the barrier layer in place of $Ga_{1-x}Al_xSb$ and firstly we focus on the investigation of the one-period model, which consists of a five-constitute symmetrized structure—AlSb/InAs/$Ga_{1-x}In_xSb$/InAs/AlSb. The basic structure parameters defined in this paper are: AlSb (4 nm)/InAs (2 nm)/$Ga_{0.7}In_{0.3}Sb$ (3 nm)/InAs (2 nm)/AlSb (4 nm). In our calculation with the FEM,[17] band structures can be obtained.

Table 2. Comparison of $E_{\rm p}$ between Ref. [14] and this paper.

	InAs	GaSb	AlSb	InSb
$E_{\rm p}$/eV in Ref. [14]	21	27	18.7	23.3
$E_{\rm p}$/eV in this paper	19	25	18.3	20

Figure 1 shows the calculated energy levels and wavefunctions, along with conduction and valence band profiles, for the type-II 'W' structure.

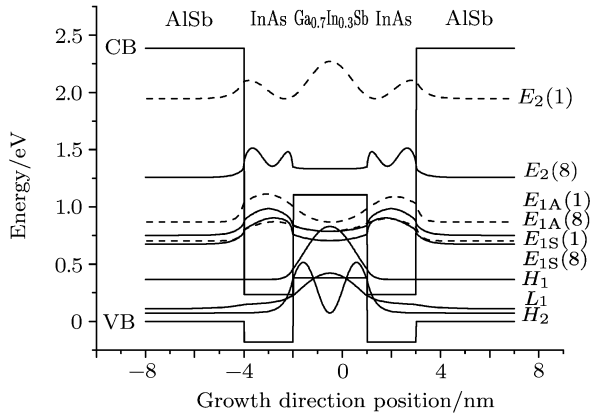


Fig. 1. Band profiles and probability density distributions of conduction bands and valence bands for the type-II 'W' quantum well, which are calculated using the eight-band $\boldsymbol{k}\cdot\boldsymbol{p}$ model (solid lines). In addition, conduction band structures are recalculated using a one-band $\boldsymbol{k}\cdot\boldsymbol{p}$ model (dashed lines).

It is well known that a broken gap alignment causes electrons and holes to separate from each other spatially—electrons are confined mainly in InAs layers while holes in the $Ga_{1-x}In_xSb$ layer, and the wavefunction overlap governs interband optical coupling, which directly contributes to the performance of lasers. In our calculation, the wavefunction overlap integral accounts for 18.8%, which is not optimal. This is because the parameters we used for the structure are non-optimal and need modifying.

According to the fundamental band gap and $\lambda = \frac{1.24}{E_{\rm g}}$, we are able to obtain the wavelengths which are shown in Fig. 2(a). The calculated wavelength is 3.77 μm. For comparison, we change the thicknesses of InAs and $Ga_{1-x}In_xSb$ separately and recalculate the wavelength. Figure 2(a) shows the wavelengths for different thicknesses. It is obvious that the wavelength becomes longer as the thickness of InAs ($Ga_{1-x}In_xSb$) layer increases. We also note that any change in the InAs layer will have an effect on electron wavefunctions, while variation in the $Ga_{1-x}In_xSb$ layer greatly affects hole wavefunctions. Figure 2(b) exhibits our simultaneously calculated corresponding wavefuction overlap integrals, which show that the increasing thickness is accompanied by a diminishing overlap. Figure 3 displays the influence of the $Ga_{1-x}In_xSb$ alloy composition on wavelength, which shows an increasing trend with the 'In' content increasing. The $Ga_{1-x}In_xSb$ layer is compressively strained, which can help to obtain our preferable wavelength. We stop increasing the 'In' content when it reaches 0.4 in the limit of highly compressive strain.

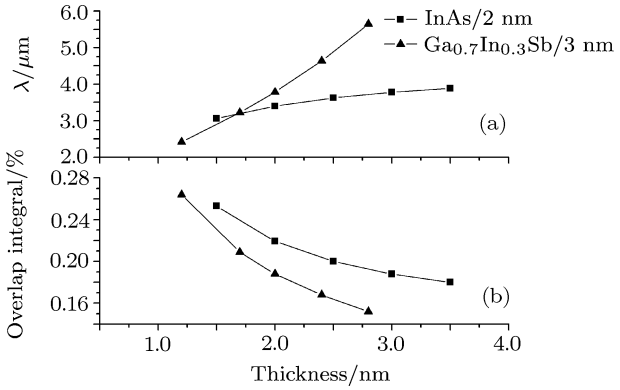


Fig. 2. Calculated wavelengths (a) and the wavefunction overlap integrals (b) through the adjustment of InAs layer and $Ga_{0.7}In_{0.3}Sb$ layer thicknesses, respectively. InAs layer thickness is fixed at 2 nm (square) while the $Ga_{0.7}In_{0.3}Sb$ thickness is variable, and $Ga_{0.7}In_{0.3}Sb$ layer thickness is fixed at 3 nm (triangle) when the InAs thickness is variable.

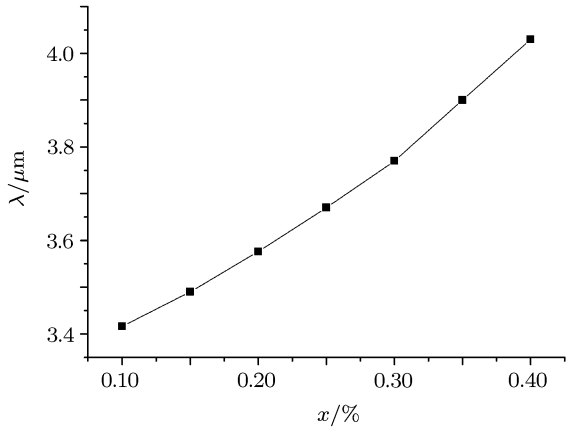


Fig. 3. Calculated wavelengths through the adjustment of the alloy composition in $Ga_{1-x}In_xSb$.

Both the eight-band model and the one-band $\boldsymbol{k}\cdot\boldsymbol{p}$ model have been widely used in the calculation of electronic band structures of materials. In comparison with eight band $\boldsymbol{k}\cdot\boldsymbol{p}$ theory, the one-band $\boldsymbol{k}\cdot\boldsymbol{p}$ model is simple because it focuses just on the conduction band while ignoring the perturbation from valence bands. Nevertheless, it is generally accepted that the one-band $\boldsymbol{k}\cdot\boldsymbol{p}$ model is still a good approximation in some cases. However, when people deal with some narrow band-gap structures, they might meet some obstacles. In order to reveal the difference between the two models in type-II 'W' QWs, we recalculate the 'W' structure using the one-band $\boldsymbol{k}\cdot\boldsymbol{p}$ model. The dashed lines in Fig. 1 show the energy levels and the wavefunctions of conduction bands obtained by the one-band $\boldsymbol{k}\cdot\boldsymbol{p}$ model, while valence bands are not involved. Comparing these results with the numerical results using the eight-band $\boldsymbol{k}\cdot\boldsymbol{p}$ model, the differences are clearly demonstrated in Fig. 1. The higher the energy level, the larger the separation between the corresponding energy levels calculated by the one-band model and the eight-band $\boldsymbol{k}\cdot\boldsymbol{p}$ model. Furthermore, note that E1S is a bit higher and the coupling of electrons between two InAs wells is larger. As expected, this consequence could be predicted and briefly attributed to the narrow band-gap, where conduction bands are perturbed strongly by valence bands.

Within the framework of one-band $\boldsymbol{k}\cdot\boldsymbol{p}$ theory, electronic (conduction band) wavefunction is composed of u_1 and u_5, which denote 'spin-up' and 'spin-down' states, respectively. However, from what we obtained in the eight-band $\boldsymbol{k}\cdot\boldsymbol{p}$ model, we disassemble the wavefunction and note that u_2 (u_6), u_3 (u_7)and u_4 (u_8) each have a considerable influence on u_1 (u_5), especially for u_4 (u_8), which means that the conduction bands are strongly coupled with the valence bands and approximately correspond to a larger effective mass in the one-band model. In addition, this directly leads to the anisotropic conduction bands shown in Fig. 4 and the different results mentioned above.

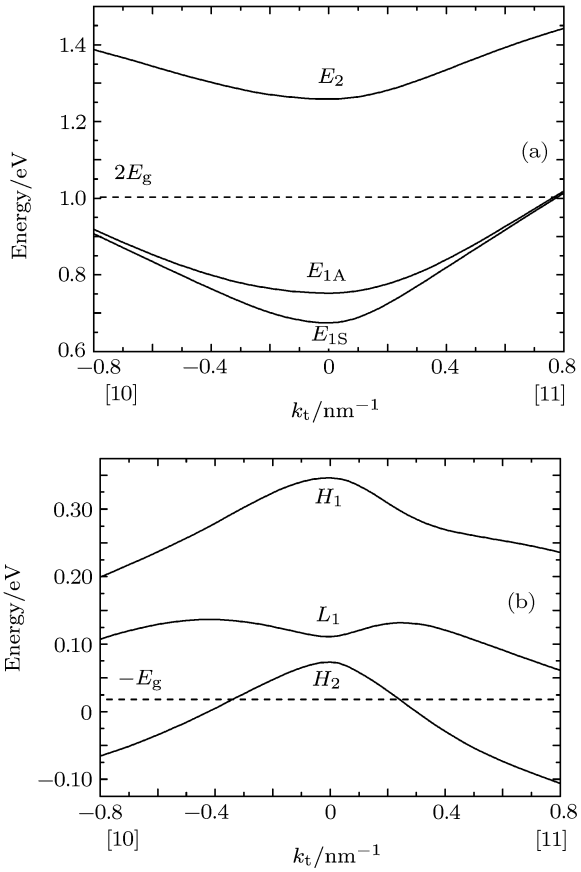


Fig. 4. Energy dispersion curves for conduction bands (a) and valence bands (b) along in-plane [11] and [10] directions. The dashed lines denote the resonant energies which equal $2E_g$ and $-E_g$, respectively.

Figure 4 shows the in-plane dispersions of both the electron and hole subband states. It is clear that the electron dispersions are approximately parabolic but still anisotropic, which is different from the result obtained by the one-band model, where the conduction bands are isotropic. Due to the compressively strained structure, the heavy hole effective mass near the Γ point tends to be smaller, which shows a similar trend to the results given by other reports.[9,18,19] In comparison with Fig. 3 in Ref. [9], where the structure consists of a $InAs/Ga_{0.75}In_{0.25}Sb$ superlattice multiple quantum well (MQW), it can be seen that the Auger recombination process is effectively eliminated in the 'W' structure due to it lacking the resonant energies for transitions in the final states, where the calculated fundamental band gap E_g ($E_{1S} - H_1$) in the type-II

'W' structure is 0.328 eV and the resonate energies which equal $2E_{\rm g}$ and $-E_{\rm g}$, respectively, are also spotted; it is also shown that the multiplicity of the valence bands contributes to an imbalance of the density of states between the conduction bands and the valence bands in superlattice MQW.[9] In the 'W' structure, however, the density of the states is more balanced, which means that the electron effective mass and hole effective mass are more balanced, thereby benefiting the improvement of the performance of laser diode.

4. Conclusion

We have presented an eight-band $\boldsymbol{k}\cdot\boldsymbol{p}$ model for the calculation of the electronic structure of type-II 'W' quantum well, which is based on InAs/$Ga_{1-x}In_xSb$/AlSb family. Considerable effects of InAs and $Ga_{1-x}In_xSb$ thickness on electronic properties have been demonstrated: an upward trend of wavelength and a downward trend of wavefunction overlap occur concurrently by increasing thickness. It has also illustrated that because of the spatial separation between electrons and holes, the variational InAs layer has a significant effect on electron wavefunction, while little influence on hole wavefunction. Meanwhile, by varying the alloy composition of $Ga_{1-x}In_xSb$, the wavelength becomes longer with 'In' content increasing. Then we compare the calculated results from the one-band $\boldsymbol{k}\cdot\boldsymbol{p}$ model with those from the eight-band $\boldsymbol{k}\cdot\boldsymbol{p}$ model, and some differences are found in the number of conduction bands in the well, the energy level as well as the shape of the wavefunction. It appears that ignoring the perturbation of valence bands in narrow band structures is not a good approximation. Nevertheless, the one - band $\boldsymbol{k}\cdot\boldsymbol{p}$ model is simple and can provide the qualitative instruction. Finally, the calculated energy dispersion curves prove that the type-II 'W' structure can effectively suppress the Auger recombination process.

Appendix

The relevant terms in the eight-band $\boldsymbol{k}\cdot\boldsymbol{p}$ model are expressed in the following forms:

$$\boldsymbol{G}_1=\begin{pmatrix} E_{\rm c} & {\rm i}Pk_x & {\rm i}Pk_y & {\rm i}Pk_z \\ -{\rm i}Pk_x & E'_{\rm v} & 0 & 0 \\ -{\rm i}Pk_y & 0 & E'_{\rm v} & 0 \\ -{\rm i}Pk_z & 0 & 0 & E'_{\rm v} \end{pmatrix}, \tag{A1}$$

$$\boldsymbol{G}_2=\begin{pmatrix} A'k_2 & Bk_yk_z & Bk_xk_z & Bk_xk_y \\ Bk_yk_z & L'k_x^2+M\left(k_y^2+k_z^2\right) & N'k_xk_y & N'k_xk_z \\ Bk_xk_z & N'k_xk_y & L'k_y^2+M\left(k_x^2+k_z^2\right) & N'k_yk_z \\ Bk_xk_y & N'k_xk_z & N'k_yk_z & L'k_z^2+M\left(k_x^2+k_y^2\right) \end{pmatrix}, \tag{A2}$$

$$\boldsymbol{G}_{\rm SO}=\frac{\Delta}{3}\begin{pmatrix} 0 & 0 & 0 & 0 \\ 0 & 0 & -{\rm i} & 0 \\ 0 & {\rm i} & 0 & 0 \\ 0 & 0 & 0 & 0 \end{pmatrix}, \tag{A3}$$

$$\boldsymbol{G}_{\rm st}=\begin{pmatrix} a_{\rm c}\left(\varepsilon_{xx}+\varepsilon_{yy}+\varepsilon_{zz}\right) & b'\varepsilon_{yz}-{\rm i}P\varepsilon_{xj}k^j & b'\varepsilon_{zx}-{\rm i}P\varepsilon_{yj}k^j & b'\varepsilon_{xy}-{\rm i}P\varepsilon_{zj}k^j \\ b'\varepsilon_{yz}+{\rm i}P\varepsilon_{xj}k^j & \{l\varepsilon_{xx}+m\left(\varepsilon_{yy}+\varepsilon_{zz}\right)\} & n\varepsilon_{xy} & n\varepsilon_{xz} \\ b'\varepsilon_{zx}+{\rm i}P\varepsilon_{yj}k^j & n\varepsilon_{xy} & \{l\varepsilon_{yy}+m\left(\varepsilon_{xx}+\varepsilon_{zz}\right)\} & n\varepsilon_{yz} \\ b'\varepsilon_{xy}+{\rm i}P\varepsilon_{zj}k^j & n\varepsilon_{xz} & n\varepsilon_{yz} & \{l\varepsilon_{zz}+m\left(\varepsilon_{xx}+\varepsilon_{yy}\right)\} \end{pmatrix}, \tag{A4}$$

$$\Gamma=\frac{\Delta}{3}\begin{pmatrix} 0 & 0 & 0 & 0 \\ 0 & 0 & 0 & 1 \\ 0 & 0 & 0 & -{\rm i} \\ 0 & -1 & {\rm i} & 0 \end{pmatrix}, \tag{A5}$$

$$E_{\rm c} = E_{\rm v} + E_0 - eV_{\rm p}, \tag{A6}$$

$$E'_{\rm v} = E_{\rm v} - \frac{\Delta}{3} - eV_{\rm p}, \tag{A7}$$

$$A' = \frac{\hbar^2}{2m_0}\left(\frac{m_0}{m_e^*} - \frac{E_{\rm p}}{E_0}\frac{E_0 + 2\Delta/3}{E_0 + \Delta}\right), \tag{A8}$$

$$P = \sqrt{\frac{\hbar^2}{2m_0}E_{\rm p}}, \tag{A9}$$

$$L' = \frac{P^2}{E_0} - \frac{\hbar^2}{2m_0}\left(\gamma_1 + 4\gamma_2\right), \tag{A10}$$

$$M = -\frac{\hbar^2}{2m_0}\left(\gamma_1 - 2\gamma_2\right), \tag{A11}$$

$$N' = \frac{P^2}{E_0} - \frac{3\hbar^2}{m_0}\gamma_3, \tag{A12}$$

$$l = 2b_{\rm v} + a_{\rm v}, \tag{A13}$$

$$m = a_{\rm v} - b_{\rm v}, \tag{A14}$$

$$n = \sqrt{3}d_{\rm v}, \tag{A15}$$

$$E_{\rm p} = \frac{3E_0\left(E_0 + \Delta\right)}{\Delta}\left(\gamma_1 - \frac{m_0}{m_{\rm SO}^*}\right), \tag{A16}$$

References

[1] Malin J I, Meyer J R, Felix C L, Lindle J R, Goldberg L, Hoffman C A, Lin C H, Chang P C, Murry S J, Yang R Q and Pei S S 1996 *Appl. Phys. Lett.* **68** 2976

[2] Yin Z Y and Tang X H 2007 *Solid-State Electron.* **51** 6

[3] Lei W and Jagadish C 2008 *J. Appl. Phys.* **104** 091101

[4] Gassenq A, Boissier G, Grech P, Narcy G, Baranov A N and Tourni é E 2009 *Electron. Lett.* **45**

[5] Hong B H, Rybchenko S I, Itskevich I E, Haywood S K, Intartaglia R, Tasco B, Rainò G and De-Giorgi M 2009 *Phys. Rev.* B **79** 165323

[6] Kim M, Canedy C L, Bewley W W, Kim C S, Lindle J R, Abell J, Vurgaftman I and Meyer J R 2008 *Appl. Phys. Lett.* **93** 191110

[7] Canedy C L, Bewley W W, Lindle J R, Kim C S, Kim M, Vurgaftman I and Meyer J R 2006 *J. Electron. Mater.* **35** 453

[8] Meyer J R, Hoffman C A, Bartoli F J and Ram-Mohan L R 1995 *Appl. Phys. Lett.* **67** 757

[9] Flatté M E, Olesberg J T, Anson S A, Boggess T F, Hasenberg T C, Miles R H and Grein C H 1997 *Appl. Phys. Lett.* **70** 3212

[10] Schliwa A 2007 *Electronic Properties of Self-organized Quantum Dots* Ph.D. Thesis (Berlin: The Technical University of Berlin)

[11] Stier O 2000 *Electronic and Optical Properties of Quantum Dots and Wires* (Berlin: Wissenschaft and Technik Verlag

[12] Foreman B A 1997 *Phys. Rev.* B **56** R 12748

[13] Burt M G 1992 *J. Phys.: Condens. Matter* **4** 6651

[14] Vurgaftman I, Meyer J R and Ram-Mohan L R 2001 *J. Appl. Phys.* **89** 5815

[15] Gu Y X, Yang T, Ji H M, Xu P F and Wang Z G 2010 *Chin. Phys.* B **19** 088102

[16] Veprek R G, Steiger S and Witzigmann B 2007 *Phys. Rev.* B **76** 165320

[17] Ram-Mohan L R and Meyer J R 1995 *J. Nonlinear. Opt. Phys.* **4** 191

[18] Chang C S and Chuang S L 1995 *IEEE J. Sel. Top. Quantum. Electron.* **1** 218

[19] Chuang S L 1991 *Phys. Rev.* B **43** 9658